Materials Chemistry and Physics 112 (2008) 696–701

Contents lists available at ScienceDirect

Materials Chemistry and Physics

journal homepage: www.elsevier.com/locate/matchemphys

Cycle mechanism and electrochemical properties of lithium manganese oxide prepared using different Mn sources

S.H. Park[a], H.S. Ahn[b], G.J. Park[c], J. Kim[d], Y.S. Lee[c,*]

[a] Energy Business Division Development Team, Samsung SDI Co. Ltd., Cheonan 330-300, Republic of Korea
[b] Korea Electrical Engineering & Science Research Institute, Seoul National University, Seoul 151-742, Republic of Korea
[c] Faculty of Applied Chemical Engineering, Chonnam National University, Gwangju 500-757, Republic of Korea
[d] Department of Materials Science and Engineering, Chonnam National University, Gwangju 500-757, Republic of Korea

ARTICLE INFO

Article history:
Received 6 April 2007
Received in revised form 28 May 2008
Accepted 15 June 2008

Keywords:
Li_2MnO_3
Composite electrode
Phase transformation
Electrochemical properties
Cathode materials
Lithium secondary battery

ABSTRACT

Li_2MnO_3 powders were synthesized using the solid-state reaction with different Mn sources (Mn_3O_4 and γ-MnOOH). The Li_2MnO_3 powders were characterized by means of XRD, SEM, TEM, and electrochemical testing. The resulting Li_2MnO_3 powders showed different physical properties and electrochemical reversible capacities depending on their synthetic temperatures and Mn sources. The obtained discharge capacities of two Li_2MnO_3 materials decreased with increasing calcination temperature. The Li_2MnO_3 synthesized using Mn_3O_4 as the starting material showed a high discharge capacity over 160 mAh g^{-1} after 25th cycle. It was found that the resulting Li_2MnO_3 powder using Mn_3O_4 was a composite consisting of monoclinic Li_2MnO_3, $LiMnO_2$, and $LiMn_2O_4$ phases. The reversible discharge capacity of Li_2MnO_3 in this study originated from the transformation between layered $LiMnO_2$ and cubic $LiMn_2O_4$ phases, which was confirmed by the differential capacity, *ex situ* XRD, and HRTEM results.

1. Introduction

Lithium containing transition metal oxides $LiMO_2$ (M = Co, Ni, Mn) and the $LiMn_2O_4$ spinel have been extensively studied as a potential cathode material for commercial lithium secondary batteries. The manganese-based oxides are promising candidates for the cathode material, because of their low cost, abundance and non-toxicity [1,2]. Lithium manganese oxide, herein referred to as the Li–Mn–O system, has three different stoichiometric compositions, viz. $LiMn_2O_4$ (cubic, $Fd3m$), $LiMnO_2$ (orthorhombic, $Pmnm$ or monoclinic, $Pm2m$), and Li_2MnO_3 (monoclinic, $C2/m$). In the case of $LiMn_2O_4$ spinel material, lithium ions are reversibly inserted into and extracted out of the host cubic spinel phase in two composition ranges, $0 \le x \le 1$ and $1 \le x \le 2$, which produce two voltage plateaus at 4 V and 3 V, respectively [3,4]. The reversible capacity of $LiMn_2O_4$ spinel material originates from the Mn^{3+}/Mn^{4+} redox reactions (the average Mn oxidation state is +3.5). The other $LiMnO_2$ layered materials form an Li_xMnO_2 system, whose average Mn oxidation state is 3+, and their electrochemical capacity originates from the Mn^{3+} to Mn^{4+} redox reaction. On the other hand, the oxidation state of Mn in Li_2MnO_3 is fixed at 4+, so that this material does not show any electrochemical reaction, because Mn^{4+} ions are very difficult to be oxidized to the Mn^{5+} state. Many research groups reported that acid treatment is very effective to obtain electrochemically active $Li_{2-x}MnO_3$ material [5,6]. Furthermore, Tabuchi et al. [7] and Numata and co-worker [8] recently reported the syntheses of $LiFeO_2$–Li_2MnO_3 and $LiCoO_2$–Li_2MnO_3 solid solutions using the hydrothermal-postannealing method and solid-state method, respectively. This showed a new way to utilize inactive Li_2MnO_3 system as a cathode material for lithium secondary battery.

In this study, the monoclinic Li_2MnO_3 was easily synthesized by a simple solid-state reaction from different Mn sources (Mn_3O_4 and γ-MnOOH) and these materials showed unexpected electrochemical reaction at room temperature. In order to reveal the unique electrochemical properties of Li/Li_2MnO_3 cell, the calcination condition was strictly controlled in the range between 500 °C and 900 °C. We report herein the various powder properties and electrochemical characterizations of the Li_2MnO_3 materials synthesized with different Mn sources.

2. Experimental

Li_2MnO_3 powders were synthesized using LiOH and two manganese sources (Mn_3O_4 and γ-MnOOH) by the solid-state reaction. $LiOH{\cdot}H_2O$ and the Mn source (cationic ratio of Li:Mn = 2:1) were simply ground and mixed using an agate mortar. Each mixture was calcined at different temperatures (500–900 °C) for 12 h in a box furnace with a heating rate of 10 °C min^{-1}.

* Corresponding author. Tel.: +82 62 530 1904; fax: +82 62 530 1909.
E-mail address: leeys@chonnam.ac.kr (Y.S. Lee).

0254-0584/$ – see front matter © 2008 Elsevier B.V. All rights reserved.
doi:10.1016/j.matchemphys.2008.06.028

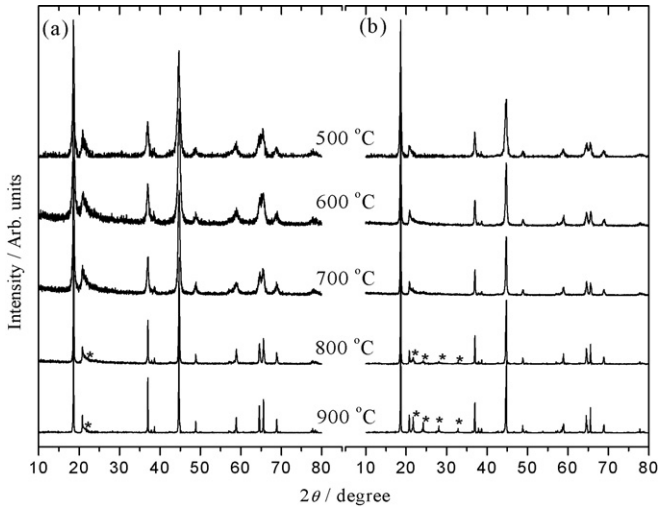

Fig. 1. X-ray diffraction (XRD) patterns of Li_2MnO_3 powders prepared using various calcination temperatures using (a) Mn_3O_4 and (b) γ-MnOOH precursor.

Powder X-ray diffraction (XRD, Rint 1000, Rigaku, Japan) using Cu Kα radiation was performed to identify the crystalline phase of the material. The particle morphologies of the resulting compound were observed using a scanning electron microscope (SEM, JSM-5300E, Japan Electron, Ltd., Japan). Transmission electron microscope (TEM, JEM 2010, JEOL, Japan) equipped with an energy-dispersive X-ray spectrometer (EDS) was employed to characterize the microstructure of the powder. The Li and Mn concentrations in the resulting materials were analyzed using an inductively coupled plasma spectrometer (ICP, SPS 7800, Seiko Instruments, Japan). The specific surface area was measured in a Gemini 2375 instrument using the Brunauer, Emmett, and Teller (BET) method.

The electrochemical characterization was performed using CR2032 coin-type cell. The cathode consisted of 20 mg of accurately weighed active material and 12 mg of conductive binder (8 mg of teflonized acetylene black (TAB) and 4 mg of graphite). It was pressed on a 200 mm^2 stainless steel mesh used as the current collector at 300 kg cm^{-2} and dried at 200 °C for 5 h in an oven. This cell consisted of a cathode and a lithium metal anode (Cyprus Foote Mineral Co.) separated by a porous polypropylene film as the separator (Celgard 3401). The electrolyte used was 1 M $LiPF_6$–ethylene carbonate (EC)/dimethyl carbonate (DMC) (1:2 by volume, Ube Chemical, Japan). The charge and discharge current density was 0.4 mA cm^{-2} with a cut-off voltage of 2.0–4.5 V at room temperature.

3. Results and discussion

The stoichiometric starting materials of Li and Mn(2:1) with different manganese sources were calcinated at various temperatures for 12 h in air atmosphere. The corresponding XRD patterns of the two Li_2MnO_3 materials using different Mn sources are shown in Fig. 1. All XRD patterns presented a monoclinic Li_2MnO_3 structure with a space group of $C2/m$. It is well known that this structure has a different cation distribution in the transition metal sites as compared with rock salt layered structures, such as $LiMO_2$ (M = Ni, Co). We expected that the Li ions occupied the 3a sites and the Li–Mn mixed cations were located at the 3b sites, which could be expressed as $[Li]_{3a}[Li_{1/3}Mn_{2/3}]_{3b}[O_2]_{6c}$ ordering. All of the XRD data clearly showed a well-developed super lattice peak at $2\theta = 20$–35°, which indicated the degree of development of the monoclinic structure of Li_2MnO_3. The XRD pattern of the Li_2MnO_3 synthesized using γ-MnOOH showed that it was better crystallized to Li_2MnO_3, where the asterisks on the peaks correspond to the development of an Mn^{4+} hexagonal network for the monoclinic Li_2MnO_3. It means that the γ-MnOOH can more easily form a Li_2MnO_3 structure and well developed at various calcination temperatures as compared with Mn_3O_4. In our previous study [11], the manganese oxide phase of the starting materials strongly affected the characteristics of the obtained pure and doped manganese oxide materials.

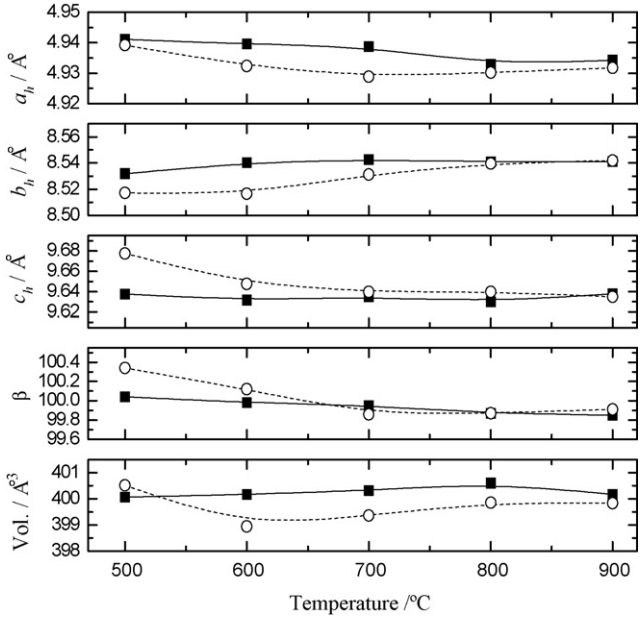

Fig. 2. Variation in the lattice constants and volume of the prepared Li_2MnO_3 powders fired at various temperatures. The filled squares and open circles represent the Li_2MnO_3 prepared using Mn_3O_4 and γ-MnOOH starting materials, respectively.

Fig. 2 shows the variation in the lattice constants of the Li_2MnO_3 powders obtained at various calcination temperatures. The filled squares and open circles represent the Li_2MnO_3 powders synthesized using Mn_3O_4 and γ-MnOOH as the starting materials, respectively. The lattice constants were calculated from the XRD data as shown in Fig. 1 by the least square method. As the calcination temperature increases, the lattice constants (a_h and c_h) decreased, whereas b_h increased. The larger lattice parameters, a_h and c_h, observed at lower calcination temperatures might be due to the presence of an oxygen rich phase, leading to the reduction of the average oxidation state of Mn in the resulting product. Moreover, the FWHM of the Li_2MnO_3 synthesized using Mn_3O_4 as the starting material at lower temperature shows more broadening than that of the Li_2MnO_3 synthesized using γ-MnOOH as the starting material.

In order to reveal the dependence of Mn starting materials in the resulting Li_2MnO_3 powder, the reaction mechanism was investigated in this study. In the case of both starting materials, external oxygen is also necessary for the formation of Li_2MnO_3 and their reaction equations are shown in the following equations:

$$2LiOH + (1/3)Mn_3O_4 + (1/3)O_2(air) \rightarrow Li_2MnO_3 + H_2O \quad (1)$$

$$2LiOH + \gamma\text{-}MnOOH + (1/4)O_2(air) \rightarrow Li_2MnO_3 + (3/2)H_2O \quad (2)$$

Therefore, the Li_2MnO_3 synthesized using Mn_3O_4 as the starting material requires more oxygen to form an ideal Li_2MnO_3 monoclinic structure. On the other hand, Li_2MnO_3 using γ-MnOOH is more easily synthesized than when used Mn_3O_4 starting material. We suggest here that it is one important fundamental reason, which induces different electrochemical and powder properties between two Li_2MnO_3 materials. Table 1 presents the chemical analysis of two resulting powders obtained at various calcination

Table 1
Chemical analysis of Li_2MnO_3 using different Mn sources

Temperature (°C)	Li_2MnO_3 using Mn_3O_4	Li_2MnO_3 using γ-MnOOH
600	$Li_2Mn_{1.10}O_{3.11}$	$Li_2Mn_{1.03}O_{3.04}$
700	$Li_2Mn_{1.06}O_{3.06}$	$Li_2Mn_{1.01}O_{3.01}$
800	$Li_2Mn_{1.04}O_{3.03}$	$Li_2Mn_{1.0}O_{2.98}$

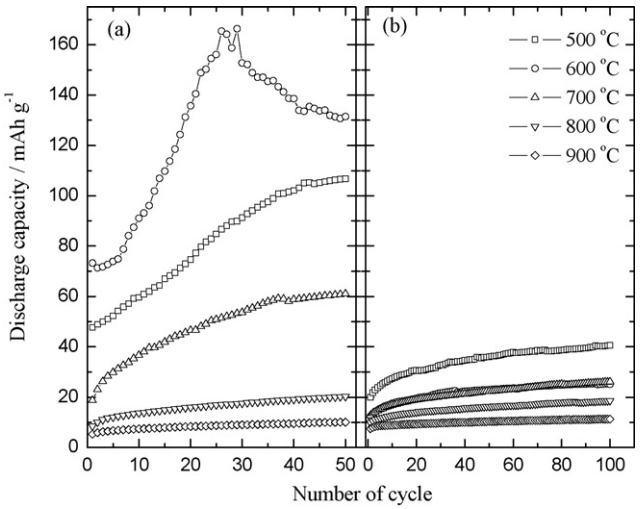

Fig. 3. Discharge capacities as a function of cycle number for Li/Li_2MnO_3 cells with various calcination temperatures: (a) using Mn_3O_4 and (b) γ-MnOOH precursor.

temperatures. This result well supports with the proposed above synthetic mechanism. The Li_2MnO_3 powder using Mn_3O_4 presents only a similar composition with stoichiometric material even though obtained at high temperature (800 °C) and the one obtained at lower temperature (600 °C) shows the typical oxygen rich compound ($LiMn_{2+x}O_{3+y}$). On the other hand, the Li_2MnO_3 using γ-MnOOH exhibits the stoichiometric composition at lower calcination temperature (600–700 °C) and the powder obtained at 800 °C shows some oxygen deficiency.

Fig. 3 shows the discharge capacity vs. the number of cycles for the $Li/LiPF_6$–EC–DMC/Li_2MnO_3 cells cycled between 2.0 V and 4.5 V with a constant current density of 0.4 mA cm^{-2}. It is well known that the ideal monoclinic Li_2MnO_3 material shows no electrochemical reaction because the charge balance of this material can be expressed as $Li_2^{1+}Mn^{4+}O_3^{2-}$. It means that the oxidation state of Mn is 4+ which makes very difficult for it to participate in the electrochemical reaction with a cut-off window of 2.0–4.5 V. The discharge capacities of the Li_2MnO_3 materials synthesized using γ-MnOOH at 500 °C, 600 °C, and 700 °C were very small and low as reported in previous studies [9,10]. However, the electrochemical capacities of the Li_2MnO_3 materials using Mn_3O_4 obtained at the same calcination temperatures showed electrochemical activity, which shows large discharge capacities on the first discharge state and these cells drastically increased capacity upon further cycling. It can be one unique result that the electrochemical characterization of Li_2MnO_3 materials depends on the sort of used starting materials during synthetic process.

It is also well known that the capacity of lithium metal oxides is strongly related to the particle properties, such as shape, particle distribution, and specific surface area [9–11]. This could be an important key technology improving and optimizing cell performance for lithium secondary battery. In order to identify the dependence for the morphological and crystalline change, SEM analysis was conducted on Li_2MnO_3 synthesized by difference of Mn_3O_4, and γ-MnOOH starting materials, respectively.

Fig. 4 shows the SEM images of the particle properties for the Li_2MnO_3 synthesized at 600 °C using Mn_3O_4 and γ-MnOOH. The powder obtained using Mn_3O_4 consisted of primarily particles of 100–200 nm diameter with a small spherical one, which is a very small particle compared with that (3–30 μm) in the previous reports [12].

However, the Li_2MnO_3 particle powder, which was obtained using γ-MnOOH remarkably increased size and well-developed needle-like particle shape, which is the typical crystalline pattern of the compound using the γ-MnOOH starting materials [11,12]. This indication could be confirmed in the SEM images shown in Fig. 4(b). It was considered that the particle size and shape of the two particles in this study were quite different, although two materials obtained at the same calcinations temperatures, which could induce various electrochemical properties during charge/discharge process. Moreover, the small particle size can be an important reason to induce the capacity increase of Li/Li_2MnO_3 using Mn_3O_4 cell during cycling, due to a large specific surface area (6.8 m^2 g^{-1}). From the above results, we concluded that Li/Li_2MnO_3 using γ-MnOOH showed a similar electrochemical characterizations compared with that of conventional Li/Li_2MnO_3, but Li/Li_2MnO_3 using Mn_3O_4 presented quite electrochemical reversibility based on the unique surface properties.

Then, what is the main reason/mechanism to induce the unique cycle property in the Li/Li_2MnO_3 using Mn_3O_4 cell? Recently, two possible mechanisms were proposed by electrochemical activity of lithium in Li_2MnO_3 structure. One of the possible reason was Li ion can be removed by non-aqueous electrolyte oxidation, which generated H^+ ions exchanged for Li^+. Also Li^+ ions can be removed by O^{2-} loss, effective removal of Li^2O. In each of two possible mechanisms electrochemical Li removal are found to operate beyond the Mn^{4+} state [13,14]. Anyway, high cut-off potential limited up 4.5 V range, therefore amount of decomposition for electrolyte was limited, which can see dQ/dV curves as shown in Fig. 5. Therefore, electrochemical capacity might occur when the discharge state

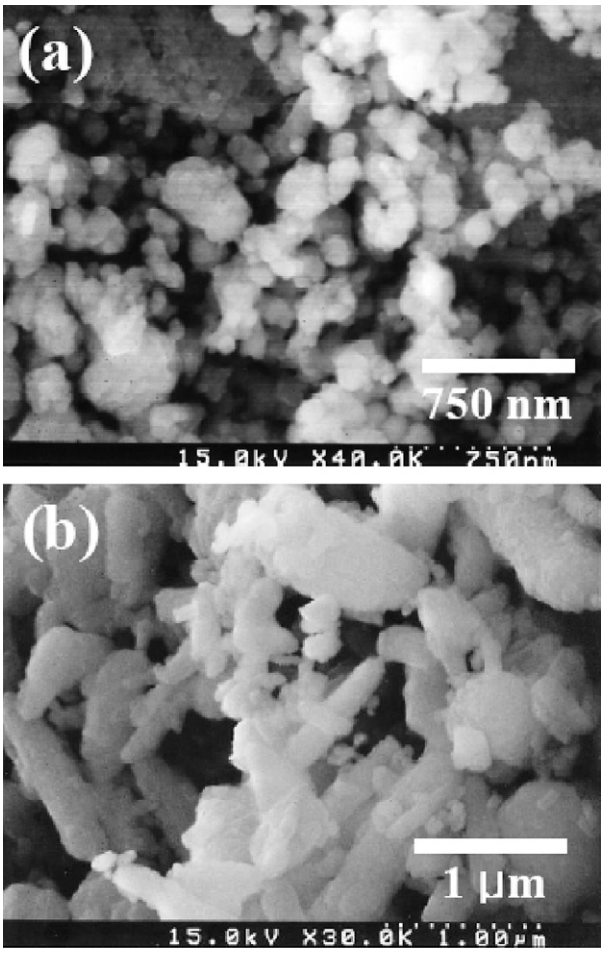

Fig. 4. SEM images of Li_2MnO_3 powders obtained at 600 °C (a) using Mn_3O_4 and (b) γ-MnOOH precursor.

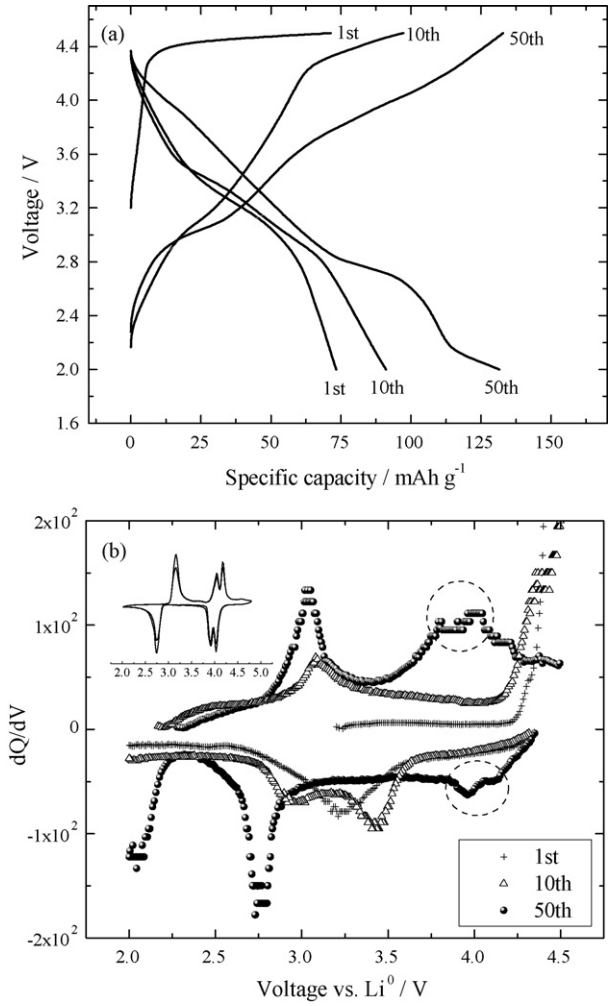

Fig. 5. (a) Charge–discharge voltage profiles of Li/Li_2MnO_3 cells prepared at 600 °C with Mn_3O_4 starting precursor, and (b) their differential capacity vs. voltage, and the inset figure is the $Li/LiMn_2O_4$ cell.

of the Li/Li_2MnO_3 cells, which was related to reduction and/or oxidation of Mn ions between 4+ and 3+ during electrochemical cycling. Also we can see that the shape of charge/discharge curves might be concerned with both spinel ($LiMn_2O_4$) and layered (orthorhombic or monoclinic $LiMnO_2$) types, respectively. As shown in Fig. 5, the charge/discharge curves present three distinct regions, which consist of spinel ($LiMn_2O_4$), spinel + layered, and layered (orthorhombic or monoclinic $LiMnO_2$) types, respectively. The initial discharge curves in the 4 V regions might involve the participation of the spinel and layered type composite electrodes. Moreover, the diagonal shape of the voltage curve between 4 V and 3 V is associated with the typical Li_xMnO_2 (O3 type layered) or orthorhombic $LiMnO_2$ electrode structure [15,16]. As lithium ions are inserted into the host structure, the voltage profiles undergo another plateau at around 3 V. The 3 V plateau is one of the characteristic features of the spinel $Li_{1+x}Mn_2O_4$ structure, in which lithium ions are inserted into the octahedral sites. Notice that the 4 V and 3 V plateaus become increasingly flatter on further cycling, which suggests that the structure has slowly transformed into a spinel structure. This observation agrees well with the previous reports that the layered Li_xMnO_2 was transformed to the spinel phase during insertion/extraction of lithium ions [17,18]. It is speculated that the increased electrochemical capacity of the Li/Li_2MnO_3 cell obtained using Mn_3O_4 can be partly attributed to the formation of a composite structure, which can be assumed by the $0.6Li_2MnO_3$–$0.4LiMn_2O_4$ electrode by theoretical calculation. Fig. 5(b) shows the differential capacity vs. voltage profiles of the Li/Li_2MnO_3 cells at various cycles and that of the spinel $Li/LiMn_2O_4$ cell is presented in the inset of Fig. 5(b) for comparison. The differential capacity of the Li/Li_2MnO_3 cell has only one redox peak in the first cycle, as can be seen from Fig. 5(b). However, this single redox peak gradually divides into two redox peaks in the 3 V and 3.5 V regions, respectively. Moreover, each of these peaks is further moved at higher voltage regions at around 4 V peaks dividing after the 50th cycle, which might well match on the normal spinel $LiMn_2O_4$ properties with two clear redox couples at 3.95 V and 4.1 V as shown in inset figure. Accordingly, these results indicate that the insertion/extraction of lithium ions occurs in a multi-stage process and that phase transitions occur from a layered to cubic spinel structure.

In order to identify the structural changes of the Li/Li_2MnO_3 obtained using Mn_3O_4 cells, it was performed *ex situ* XRD measurements after cycling. To investigate the structural difference of the cathode before and after cycling, each tested cell was left in a glove box for 2 days to reach equilibrium after the cycling. The electrodes after cycling were washed with DMC solution to remove $LiPF_6$ salt. Fig. 6 shows the *ex situ* XRD patterns of each cycled electrode after various cycling. The phase transitions occurred after the first cycle for the Li_2MnO_3 host material, followed by the appearance of another phase at a lower angle. Moreover, the fraction of the original phase considerably decreased after the 30th cycle, whereas that of the newly formed phase increased, as can be seen in Fig. 6. Especially, the super lattice structure peaks at around $2\theta = 20$–$25°$ almost disappeared after the 50th cycle, which means that an irreversible phase transformation occurred due to the electrochemical reaction of the electro-active Li_2MnO_3. Unfortunately, it is impossible to define structural refinements clearly, due to the lower crystallinity. However, we could find that this new structure might consist of $Li_xMn_2O_4$ and $LiMnO_2$ (O_3 type or orthorhombic) structures.

The microstructures of the as-prepared materials and cycled electrodes were examined using transmission electron microscopy (HRTEM), as shown in Fig. 7. In agreement with the *ex situ* XRD result and electrochemical analysis, the electron diffraction pattern of the as-prepared particles indicated that the main phase is Li_2MnO_3. We also found small fractions of $LiMnO_2$ and $LiMn_2O_4$ phases in the as-prepared particles. However, after charge/discharge cycling, the sub-phases in the cycled electrodes

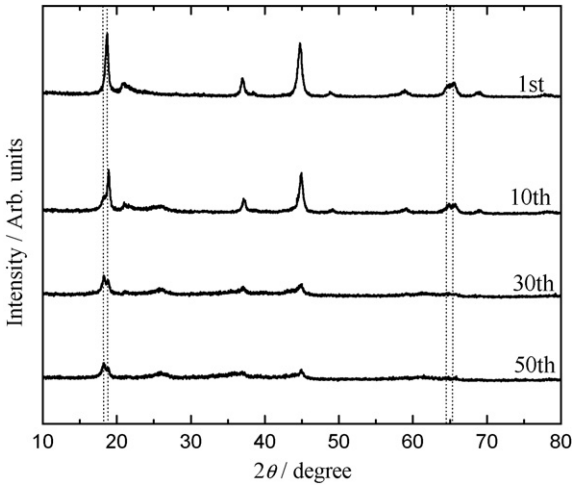

Fig. 6. *Ex situ* XRD patterns of Li_2MnO_3 electrode prepared at a calcination temperature of 600 °C. All of the electrodes were carefully disassembled after each cycle in an argon filled glove box.

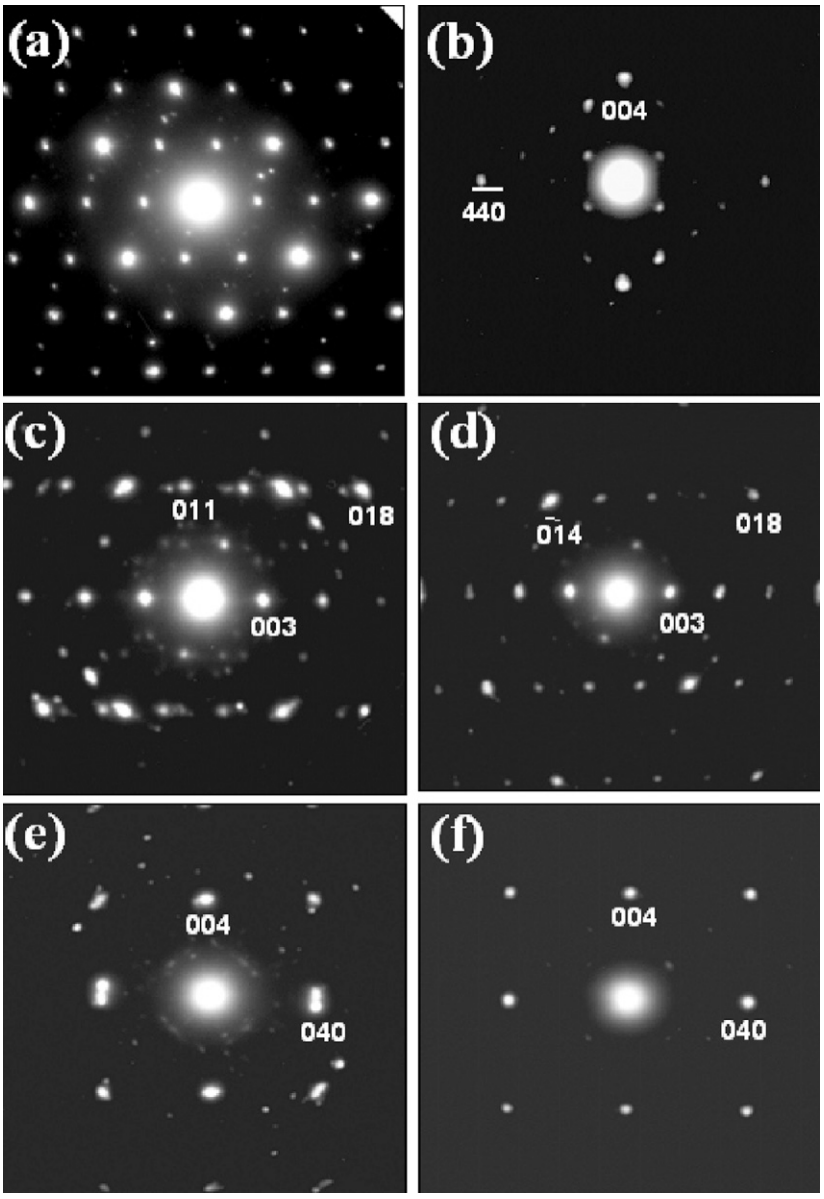

Fig. 7. SAD patterns (zone 1 0 0) of Li_2MnO_3 electrode obtained at 600 °C. (a), (c) and (e) were obtained before the cycling of the electrode, and indicated the presence of Li_2MnO_3, $LiMnO_2$, and $LiMn_2O_4$ phases, respectively; (b), (d) and (f) were obtained after the cycling of the electrode, and indicated the presence of Li_2MnO_3, $LiMnO_2$, and $LiMn_2O_4$ phases, respectively.

contained a small fraction of $LiMnO_2$ and $LiMn_2O_4$ phases. We are unsure of the exact fraction of the tetragonal phase, which resulted from the transformation of spinel $LiMn_2O_4$ phase, due to the limited number of particles examined using TEM. However, we believe that the fraction should be negligible, since the XRD data did not show presence of appreciable amount of the layered $LiMnO_2$ and $LiMn_2O_4$ spinel phases. The diffraction patterns indicate that the defected Li_2MnO_3 structure may also be transformed into the $LiMnO_2$ and $LiMn_2O_4$ symmetry. We suggested that the observed electrochemical capacity in the Li/Li_2MnO_3 cell might have been brought about by the presence of impurity phase, such as partially ordered $LiMnO_2$ and $LiMn_2O_4$ phases in the resulting material.

4. Conclusion

Monoclinic Li_2MnO_3 powders were prepared by the solid-state reaction using Mn_3O_4 and γ-MnOOH precursors. The Li_2MnO_3 synthesized using different starting materials and calcination temperatures showed different structural properties, surface morphologies, and electrochemical reversible capacities. The Li_2MnO_3 synthesized using γ-MnOOH was better crystallized than that synthesized using Mn_3O_4, because of the development of Mn^{4+} ions in the monoclinic Li_2MnO_3 structure. According to the *ex situ* XRD, differential capacity analysis, and HRTEM study, the Li_2MnO_3 material synthesized using Mn_3O_4 at 600 °C was mainly composed of Li_2MnO_3, sub-$LiMnO_2$, and sub-$LiMn_2O_4$ phases. Moreover, the Li/Li_2MnO_3 cell was gradually transformed between the $LiMnO_2$ and $LiMn_2O_4$ phases during cycling (2.0–4.5 V).

Acknowledgement

This work was supported by Korea Electrical Engineering & Science Research Institute by Korea Government (2007).

References

[1] F. Capitaine, P. Gravereau, C. Delmas, Solid State Ionics 89 (1996) 197.
[2] A.R. Armstrong, P.G. Bruce, Nature 381 (1996) 499.
[3] T. Ohzuku, M. Kitagawa, T. Hirai, J. Electrochem. Soc. 137 (1990) 769.
[4] M.M. Thackeray, J. Electrochem. Soc. 142 (1995) 2558.
[5] Y. Shao-Horn, Y. Ein-Eli, A.D. Robertson, W.F. Averill, S.A. Hackney, W.F. Howard Jr., J. Electrochem. Soc. 145 (1998) 16.
[6] C.S. Johnson, S.D. Korte, J.T. Vaughey, M.M. Thackeray, T.E. Bofinger, Y. Shao-Horn, S.A. Hackney, J. Power Sources 81–82 (1999) 491.
[7] M. Tabuchi, A. Nakashima, H. Shigemura, K. Ado, H. Kobayashi, H. Sakaebe, H. Kageyama, T. Nakamura, M. Kohzaki, A. Hirano, R. Kanno, J. Electrochem. Soc. 149 (2002) A509.
[8] K. Numata, S. Yamanaka, Solid State Ionics 118 (1999) 117.
[9] P. Strobel, B. Lambert-Andron, J. Solid State Chem. 75 (1988) 90.
[10] W. Tang, H. Kanoh, K. Ooi, Y. Wang, J. Mater. Sci. Lett. 19 (2000) 1361.
[11] Y.S. Lee, C.S. Yoon, Y.K. Sun, M. Yoshio, Electrochem. Solid State Lett. 5 (1) (2002) A1.
[12] Y.S. Lee, M. Yoshio, Electrochem. Solid State Lett. 4 (10) (2001) A166.
[13] A.D. Robertson, P.G. Bruce, Chem. Mater. 15 (2002) 1984.
[14] R. Armstrong, P.G. Bruce, Electrochem. Solid State Lett. 7 (1) (2004) A1.
[15] Y.-I. Jang, B. Huang, Y.-M. Chiang, D.R. Sadoway, Electrochem. Solid State Lett. 1 (1998) 13.
[16] T.E. Quine, M.J. Duncan, A.R. Armstrong, A.D. Robertson, P.G. Bruce, J. Mater. Chem. 10 (2000) 2838.
[17] G. Vitins, K. West, J. Electrochem. Soc. 144 (1997) 2587.
[18] Y. Shao-Horn, S.A. Hackney, A.R. Armstrong, P.G. Bruce, R. Gitzendanner, C.S. Johnson, M.M. Thackeray, J. Electrochem. Soc. 146 (1999) 2404.